SUPPLEMENTARY INFORMATION: Resonance Raman Optical Activity Shows Unusual Structural Sensitivity for Systems in Resonance with Multiple Excited States: Vitamin B_{12} Case

*Ewa Machalska,[1,2] Grzegorz Zajac,[2] Anna Gruca,[1,2], Fabio Zobi,[3] Malgorzata Baranska,[1,2] Agnieszka Kaczor,[*1,2]*

[1] Faculty of Chemistry, Jagiellonian University, Gronostajowa 2, Krakow 30-387, Poland

[2] Jagiellonian Centre for Experimental Therapeutics (JCET), Jagiellonian University, Bobrzynskiego 14, Krakow 30-348, Poland

[3] Department of Chemistry, University of Fribourg, Chemin du Musée 9, 1700 Fribourg, Switzerland

EXPERIMENTAL

Materials

Cyanocobalamin (CNCbl) and hydroxocobalamin (OHCbl) chloride were purchased from Sigma-Aldrich. 1,4-diethynylbenzenecobalamin (HC≡C-Ph-C≡CCbl) and a cobalamin ring derivative (CNCbl-Br) were synthesized *via* reported procedures.[1] Studied derivatives are characterized chemically elsewhere.[1,2]

Spectroscopic measurements (UV-Vis/ECD, Raman/ROA)

Raman and ROA spectra of all compounds dissolved in distillated water (c=0.1 mg/mL) were measured using a Chiral*RAMAN-2X* spectrometer (*BioTools Inc.*) at a resolution of 7 cm^{-1} in the range of 2500-250 cm^{-1} employing the excitation wavelength of 532 nm. The solutions were measured in ROA quartz optical cells with anti-reflective coating. Laser power of 200 mW, integration time of 4.0424 s and 24 hour (CNCbl, OHCbl) or 72 hour (CNCbl-Br, HC≡C-Ph-C≡CCbl) acquisition time were used for ROA and Raman measurements of studied solutions. For CNCbl-Br and HC≡C-Ph-C≡CCbl a longer accumulation time was used, due to the insufficient S/N ratio after 24 h acquisition. Due to the limited stability of CNCbl-Br (24 h) and HC≡C-Ph-C≡CCbl (12 h) under laser irradiation, the final 72 hour spectra were averaged over three 24 h measurements (CNCbl-Br) and six 12 h (HC≡C-Ph-C≡CCbl) of freshly prepared samples. Before measurements, to remove physical impurities, all solutions were purified by using MilliporeTM Millex® syringe PTFE filters (pore size 0.45 μm). ROA and Raman spectra were corrected by subtracting the spectrum obtained for the solvent using OPUS software. Baseline of solvent-corrected spectra were then subtracted by asymmetric last squares smoothing method, and then, smoothed with the ten-point Savitzky–Golay procedure using OriginPro software.

For cobalamins, 24 h-72 h acquisition time were used typically to obtain RROA spectra with a high S/N ratio. In fact, the most intense RROA bands of cobalamins can be recorded easily in 30 minutes (Figure S1).

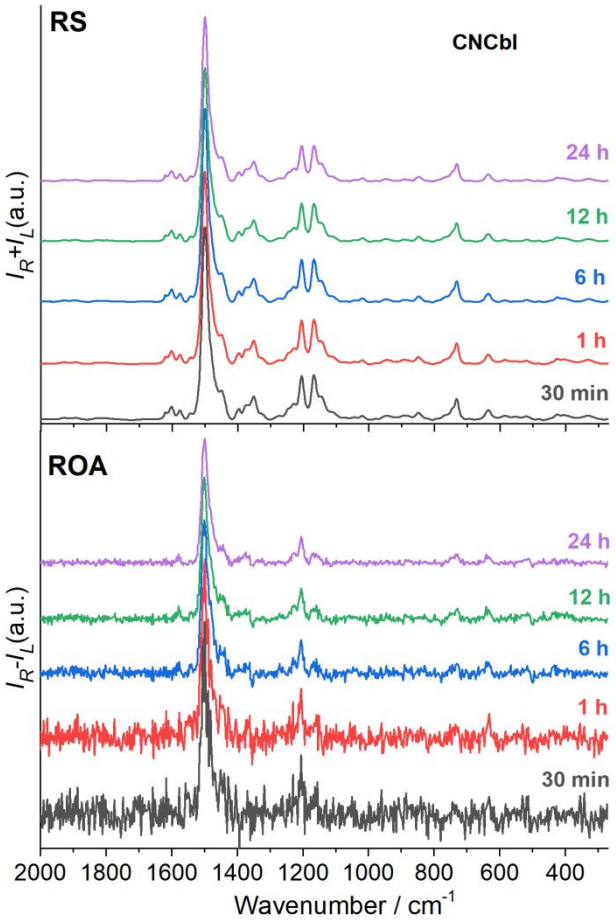

Figure S1. Comparison of RROA spectra of CNCbl recorded in 30 min, 1 h, 6 h, 12 h and 24 h.

UV-Vis and ECD spectra were recorded in the 220-700 nm spectral range using quartz cells with a path length of 10 mm, a scanning speed of 100 nm/min, a bandwidth of 1 nm, 0.5 s response time by accumulation of a single scan on a Jasco J-815 spectrometer. The concentration of all samples was 0.1 mg/mL. Obtained spectra were solvent and baseline corrected using JASCO software.

Stability of cobalamins in RROA experiment

To prove that local heating and photochemical degradation do not occur, even after prolonged irradiation with the ROA laser, the ECD spectra were registered after RROA measurements (Figure S2). The ECD spectra registered after the ROA measurements are unchanged compared to the ECD spectra of the freshly prepared solutions of cobalamins proving that studied cobalamins are photostable in the conditions of the experiment.

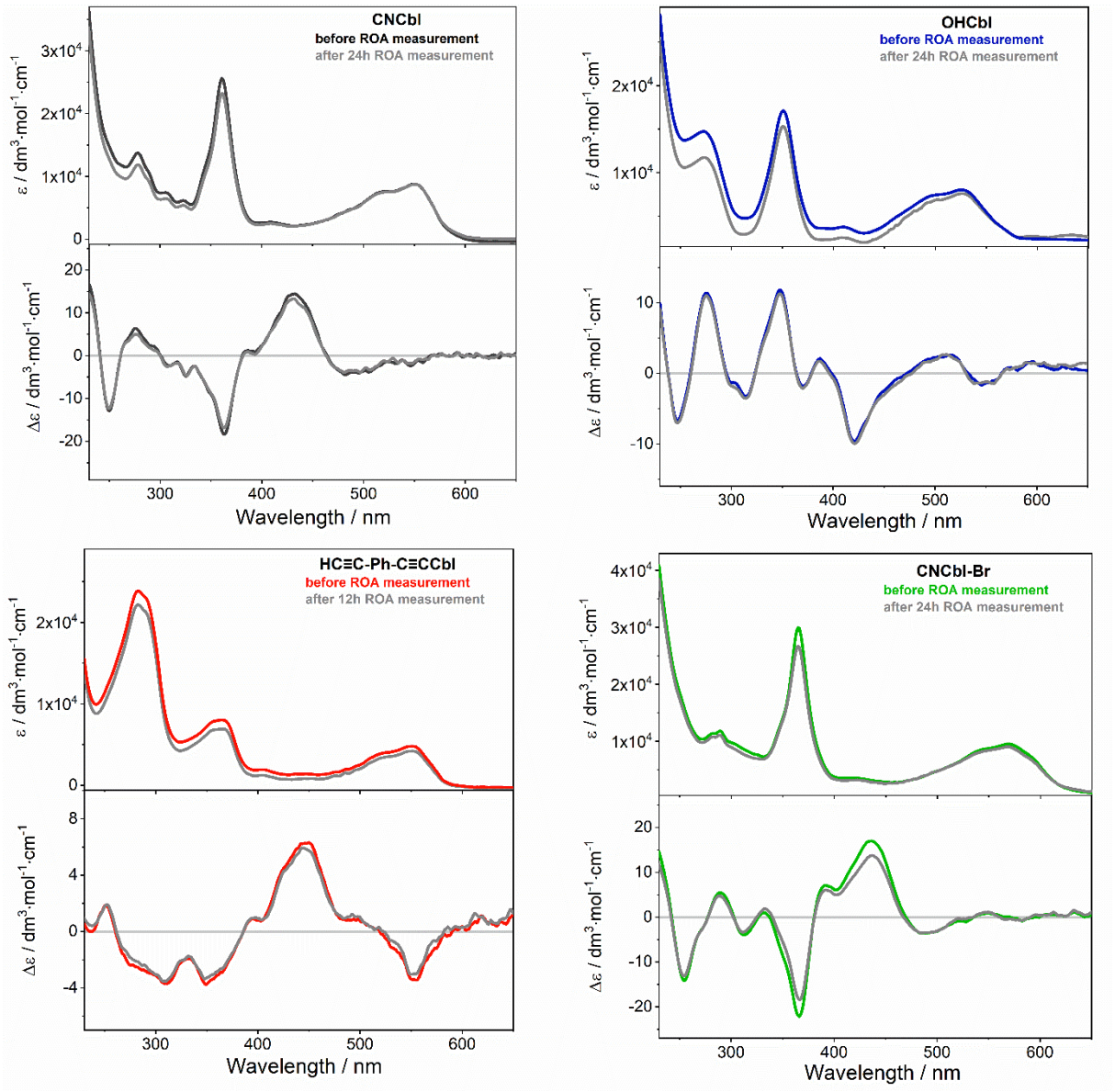

Figure S2. The ECD spectra of studied cobalamins recorded before and after RROA experiments involving prolonged irradiation with the RROA laser.

Quantum-chemical calculations

Quantum chemical calculations of spectroscopic properties, mainly Raman and ROA spectra of one of the studied cobalamins (CNCbl) were carried out for qualitative rationalization of obtained experimental spectra. However, we considered only Raman/ROA calculation in pre-resonance conditions in use of standard frequency-dependent Raman calculations in Gaussian, despite the fact that using excited lines of very close energy to the calculated electronic transitions can lead to meaningless results. We used two DFT hybrid functionals: a common B3LYP functional, and its modification with long range correction: CAM-B3LYP, combined with 6-31G(d) basis set, as well as MDF10 pseudopotential and basis set for Co. Only the CAM-B3LYP functional showed satisfying agreement with all experimental spectra (UV-Vis/ECD, Raman/ROA and will be referred to below.

DFT calculations were performed by means of Gaussian 09 E.01 package.[3] Crystallographic structure of cyanocobalamin[4] was optimised at the CAM-B3LYP/6-31G(d) theory level for H, C, O, N and P atoms, and using the MDF10 pseudopotential and basis set for Co atom (Figure S3). The solvent (water) was modelled using the CPCM model. The entire structure of CNCbl was preserved in the geometry optimization and spectroscopic calculations. The optimized geometry did not change significantly in respect to the X-ray structure, that was reflected in the small change of the corrin ring fold angle described as the angle between two planes: N21-C4-C5-C6-N22-C9-C10 and C10-C11-N23-C14-C15-C16-N24 from 14.0° in X-ray to 17.1° after CAM-B3LYP/MDF10/6-31G(d)/CPCM optimization Figure S4.

The optimised CNCbl structure (Figure S4 and Table S1) was then submitted to the TD-DFT calculations of vertical electronic absorption energies and intensities (oscillatory and rotatory strengths of first 100 singlet excited states) as well as frequency calculations at the same level of theory along with calculation of pre-resonance Raman and ROA intensities using the frequency-dependent CPHF procedure, at 470 nm of incident light wavelength (Table S2). The incident light wavelength (470 nm) used in the Raman/ROA calculations was downshifted in comparison to the experimental one (532 nm), due to the downshift of the theoretical energy transition of interest in respect to the experimental spectra. We studied also other incident light lines in the α/β spectral region, but the 470 nm resulted in the best agreement of the experimental and calculated spectra. Comparison of the theoretical Raman/ROA profiles, obtained using selected excitation lines are presented in Figure 3 (manuscript). UV-Vis/ECD and Raman/ROA curves were obtained by a convolution with the Gaussian functions of 0.1 eV and 6 cm^{-1} half width at half maximum, respectively employing GaussView 6 software.[5] Further analysis of molecular orbitals involved in the electronic transitions was performed by means of GaussSum 3 software.[6] Calculated Raman/ROA frequencies were multiplied by a single factor of 0.9446 to fit to the experimental ones.

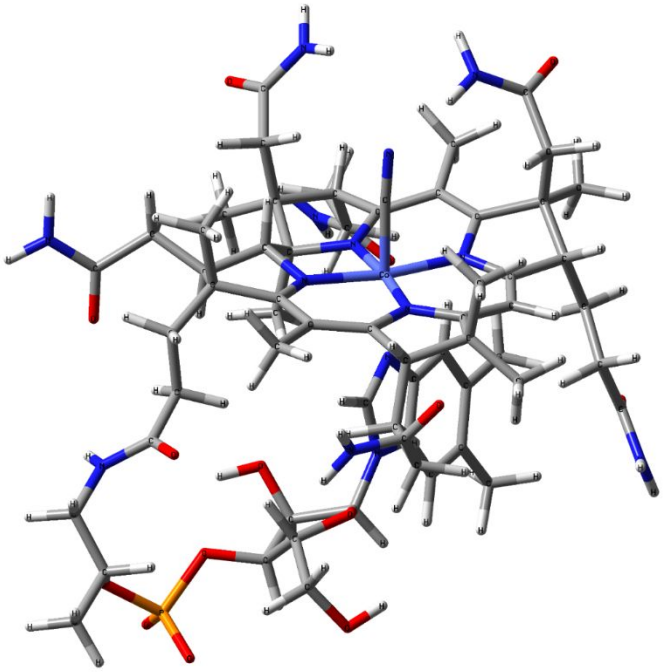

Figure S3. The structure of CNCbl, optimized at CAM-B3LYP/6-31G(d)/MDF10/6-31G(d)/PCM level.

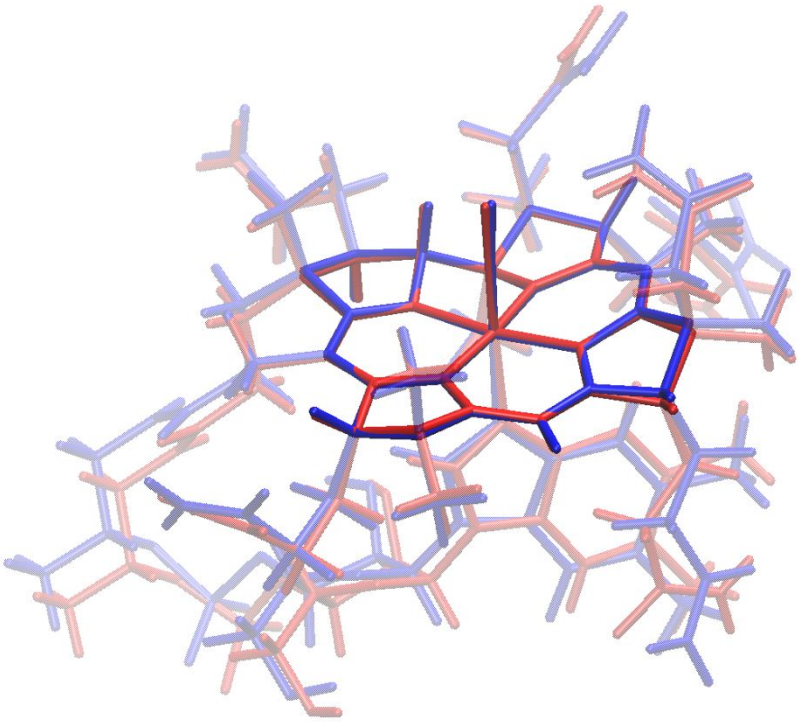

Figure S4. Comparison of the X-ray structure (blue) and the optimized geometry of CNCbl (red) calculated at CAM-B3LYP/6-31G(d)/MDF10/6-31G(d)/PCM theory level (full color – corrin ring, transparent – all other atoms).

Table S1. The Cartesian coordinates of the optimized geometry of CNCbl at CAM-B3LYP/6-31G(d)/MDF10/PCM level.

Atom No	Symbol	x / Å	y / Å	z / Å	Atom No	Symbol	x / Å	y / Å	z / Å
1	Co	0.000000	0.000000	0.000000	92	C	4.997812	2.416952	0.793380
2	P	7.685313	1.117502	5.058308	93	H	4.690516	3.200313	1.489904
3	C	-0.148403	2.707870	1.009340	94	H	4.493914	1.491149	1.089505
4	C	-1.277630	3.824110	0.998966	95	C	6.487342	2.151143	0.886042
5	C	-2.535807	3.003743	1.436276	96	C	2.106140	4.963094	-0.375346
6	H	-3.417865	3.386350	0.921040	97	H	1.933886	5.160476	-1.435564
7	C	-2.205301	1.626134	0.906533	98	H	1.247467	5.382919	0.155470
8	C	-3.221218	0.630050	0.613574	99	C	3.306066	5.740041	0.149561
9	C	-2.882886	-0.659683	0.320654	100	C	-0.649116	0.388484	-1.723550
10	C	-3.818115	-1.839343	-0.016105	101	C	8.637081	2.872012	1.812348
11	C	-2.883478	-3.036607	0.330243	102	H	9.043180	3.838456	2.122249
12	H	-3.083876	-3.888974	-0.326069	103	H	9.097355	2.596188	0.860390
13	C	-1.539275	-2.434815	0.035488	104	C	8.976104	1.815187	2.856819
14	C	-0.463005	-3.175998	-0.430349	105	H	8.535474	0.866526	2.539444
15	H	-0.628747	-4.235454	-0.570153	106	C	10.474638	1.656645	3.043728
16	C	0.750648	-2.655483	-0.856367	107	H	10.922742	2.602175	3.366444
17	C	1.773518	-3.471603	-1.620418	108	H	10.955099	1.344659	2.110986
18	C	3.030176	-2.576265	-1.489077	109	H	10.665087	0.899540	3.807069
19	H	3.549658	-2.554465	-2.447998	110	C	3.534332	-1.412708	3.907039
20	C	2.430523	-1.209596	-1.180405	111	H	3.418645	-2.143373	4.713446
21	C	3.122844	-0.028573	-1.264749	112	C	4.153017	-0.115888	4.436810
22	C	2.535261	1.225346	-0.826174	113	H	3.870829	0.068560	5.479410
23	C	3.131537	2.636793	-1.012616	114	C	5.646019	-0.393110	4.254776
24	C	2.201419	3.469437	-0.072302	115	H	6.038399	-0.984186	5.085623
25	H	2.592114	3.374788	0.942724	116	C	5.684787	-1.228136	2.971095
26	C	0.889174	2.690529	-0.145708	117	H	5.782360	-0.568070	2.102687
27	H	0.369519	2.928383	-1.077602	118	C	6.776470	-2.283235	2.957299
28	C	0.578838	2.613023	2.356105	119	H	6.815178	-2.767806	1.971944
29	H	-0.100366	2.329193	3.160388	120	H	7.735541	-1.796784	3.148472
30	H	1.031366	3.572377	2.613990	121	C	1.981467	-0.769578	2.070739
31	H	1.374500	1.869919	2.319829	122	H	2.772866	-0.640220	1.352312
32	C	-0.978509	5.020795	1.904051	123	C	-1.282827	-0.728668	3.437566
33	H	-1.752992	5.776583	1.776388	124	H	-2.035575	-0.363832	2.753006
34	H	-0.026337	5.490432	1.643983	125	C	-1.651910	-1.120084	4.714966
35	H	-0.922263	4.741151	2.956608	126	C	-0.678941	-1.601890	5.632857
36	C	-1.542734	4.312426	-0.453831	127	C	0.657199	-1.657544	5.268703
37	H	-0.718767	4.947385	-0.791317	128	H	1.403021	-2.005381	5.975631
38	H	-1.587885	3.456552	-1.132078	129	C	1.004619	-1.264635	3.977633
39	C	-2.814062	5.135916	-0.624305	130	C	0.056004	-0.822082	3.050436
40	C	-2.903331	2.934198	2.936449	131	C	-3.102800	-1.068703	5.116515
41	H	-3.415778	1.990536	3.140096	132	H	-3.493436	-2.082570	5.254357
42	H	-2.008006	2.918943	3.561370	133	H	-3.704537	-0.578125	4.346693
43	C	-3.827786	4.061275	3.388211	134	H	-3.249647	-0.523018	6.054293
44	H	-3.352138	5.040226	3.289835	135	C	-1.102712	-2.069331	7.000008
45	H	-4.720691	4.086544	2.750079	136	H	-1.600693	-1.274174	7.565467
46	C	-4.301842	3.854265	4.818570	137	H	-0.244154	-2.410853	7.583065
47	C	-4.644412	1.143536	0.599740	138	H	-1.813193	-2.899875	6.922343
48	H	-4.715969	2.052253	-0.004786	139	N	2.224030	-1.221183	3.317143
49	H	-5.008296	1.388669	1.603392	140	N	0.705950	-0.536129	1.847668
50	H	-5.336456	0.435782	0.160895	141	N	-0.935335	1.470648	0.741670
51	C	-5.162160	-1.944721	0.713319	142	N	-1.565839	-1.112750	0.217893
52	H	-5.493403	-2.987319	0.687246	143	N	1.132781	-1.380423	-0.728047
53	H	-5.940372	-1.365139	0.222761	144	N	1.357422	1.297306	-0.287858
54	H	-5.088827	-1.639471	1.759514	145	N	-3.722792	4.616377	-1.482701
55	C	-4.028522	-1.875830	-1.562908	146	H	-4.553176	5.154405	-1.690311
56	H	-3.056441	-1.937058	-2.060909	147	H	-3.535182	3.800681	-2.045818

57	H	-4.576611	-2.793915	-1.794283	148	N	-4.673679	4.978040	5.470799
58	C	-4.842798	-0.730421	-2.145623	149	H	-5.069853	4.899739	6.396651
59	C	-2.983092	-3.499149	1.798523	150	H	-4.659380	5.885892	5.031642
60	H	-2.847656	-2.646358	2.467431	151	N	-4.152640	0.197176	-2.838544
61	H	-3.992093	-3.875664	1.975912	152	H	-4.664848	0.987137	-3.207170
62	C	-1.988300	-4.586807	2.184358	153	H	-3.138458	0.214325	-2.900751
63	H	-2.094477	-5.464359	1.534876	154	N	-1.374135	-6.056177	4.011631
64	H	-0.956175	-4.240160	2.061714	155	H	-1.421342	-6.385435	4.965051
65	C	-2.163112	-5.025783	3.631369	156	H	-0.721810	-6.498610	3.382262
66	C	1.332792	-3.491280	-3.100314	157	N	6.636870	-3.440983	-2.308733
67	H	1.221938	-2.477988	-3.499491	158	H	7.023654	-3.407917	-3.241741
68	H	0.378916	-4.013140	-3.217565	159	H	7.171067	-3.033468	-1.556327
69	H	2.092405	-4.013058	-3.689517	160	N	7.210580	3.031878	1.605861
70	C	1.906315	-4.914213	-1.134472	161	H	6.724927	3.730371	2.147857
71	H	2.681993	-5.417740	-1.714562	162	N	3.736242	6.751559	-0.631618
72	H	0.971834	-5.458742	-1.294049	163	H	4.478210	7.349319	-0.294819
73	H	2.154675	-4.978874	-0.071913	164	H	3.284206	6.994504	-1.499995
74	C	4.048336	-2.942052	-0.383438	165	N	-1.096352	0.578607	-2.780173
75	H	3.531887	-3.121661	0.564502	166	O	6.342048	0.823490	4.099777
76	H	4.677698	-2.065421	-0.211722	167	O	8.374619	2.230453	4.089684
77	C	4.978720	-4.139617	-0.669401	168	O	7.261217	1.828071	6.301880
78	H	5.806417	-4.104504	0.045792	169	O	8.482173	-0.151065	5.100498
79	H	4.461740	-5.086099	-0.521032	170	O	-3.015672	6.190847	-0.031435
80	C	5.501911	-4.142666	-2.092564	171	O	-4.357820	2.744293	5.338443
81	C	4.526039	-0.038069	-1.837527	172	O	-6.064099	-0.670629	-2.002640
82	H	4.637179	0.702071	-2.632846	173	O	-2.951790	-4.488547	4.403140
83	H	4.765233	-0.998931	-2.288075	174	O	4.895939	-4.703884	-3.003288
84	H	5.295226	0.168895	-1.087062	175	O	7.006234	1.196559	0.300741
85	C	2.941844	3.014966	-2.496762	176	O	3.823856	5.473446	1.230827
86	H	1.887702	3.023976	-2.789061	177	O	4.413482	-1.909407	2.921052
87	H	3.457884	2.309687	-3.151075	178	O	3.767109	0.956558	3.607506
88	H	3.359680	4.005452	-2.695292	179	H	4.521572	1.573893	3.619770
89	C	4.614730	2.817024	-0.638788	180	O	6.576838	-3.233295	3.985330
90	H	5.242308	2.276391	-1.344241	181	H	5.693686	-3.606759	3.836409
91	H	4.857786	3.874610	-0.782421					

Table S2. Calculated and experimental frequencies of cyanocobalamin.

Calculations		**Experimental**		
Mode No	*ROA v/cm^{-1} x0.9446*	*RS v/cm^{-1}*	*ROA v/cm^{-1}*	Assignment
441	1634(–)	1622	-	C=C str (5-6), C=N str (4-21)
439	1608(+)	1602	-	C=C str (14-15), C=N str (16-24)
435	1570(+)	1577	1578(+)	C=C str (5-6;10-11), C-H bend (10), C=N str (16-24;4-21)
430	1546(+)	1543	1546(+)	C=C str (5-6;10-11;14-15), C=N str (9-22;11-23;16-24;4-21)
429	1511(+)	1501	1501(+)	C-H bend (B2), C=N str (B2-B1;B2-B3)
427	1500(+)			C=C str (5-6;9-10;14-15), C=N str (4-21;11-23;16-24), C-H bend (10), CH_3 bend asym
426	1492(+)			CH_3 bend asym, C-H bend (10), CH_2 bend (scissoring), C=C str (14-15), C=N str (16-24;9-22)
424	1476(+)			CH_3 bend asym, CH_2 bend (scissoring), C=C str (14-15)
423	1472(+)			CH_3 bend asym, CH_2 bend (scissoring)
422-386	1466-1392(+)	1452	1449(+)	CH_3 bend asym, CH_2 bend (scissoring)
385	1389(+)	1396	1398(+)	CH_3 bend sym (umbrella)
380	1380(+)			CH_3 bend sym (umbrella)
379	1379(+)			CH_3 bend sym (umbrella), CH_2 bend (scissoring)
378	1377(+)			CH_3 bend sym (umbrella), CH bend
366	1358(+)	1374	1376(+)	CH_3 bend sym (umbrella), CH bend
364	1352(+)			CH_3 bend sym (umbrella), CH bend
359-354	1335-1324(+)	1350	1344(+)	CH_2 wagg, CH bend
342	1287(–)	1316s	1310(–)	CH_2 wagg, CH bend
335	1269(+)	1275	1270(+)	CH_2 twist, CH bend
333	1259(+)			CH_2 twist, CH_2 wagg, CH bend
327	1240(+)	1247s	-	CH_2 wagg, CH_2 twist, CH bend, NH bend
320	1212(+)	1228	1228(+)	CH_2 wagg, CH bend, NH bend, CH_3 rock
317	1196(+)	1205	1205(+)	CH_2 twist, CH bend, CH_3 rock
315	1189(+)			C-C str (corr. ring), CH_2 twist, CH bend, CH_3 rock,
311	1177(+)			CH_2 twist, CH bend, CH_3 rock
304	1146(+)	1168	1168(+)	C-N str (6-22;14-23), C-C str (corr. ring), CH_2 twist, CH bend, CH_3 rock,
297	1126(+)	1145s	-	CH_2 twist, CH bend, CH_3 rock, NH_2 rock, CH bend,
289	1093(–)	1105s	1109(–)	C-N str (6-22;14-23), NH_2 rock, CH_2 twist, CH bend
266	1033(–)	1079	-	Co-N str (-22;-23), C-N str (19-24), C-C str (8-9;13-14;15-53;17-54;30-31;55-56), CH_3 rock
257	1006(+)	1045	1044(+)	C-N str (19-24), C-C str, CH_3 rock
252	988(+)	1022	1005(–)	CH_2 rock, NH_2 rock, CH_3 rock
246	952(+)	975		CH_3 rock, NH_2 rock, C-C str (48-49;11-12;12-46;12-47;49-50;13-48)
242	932(–)	945	943(+)	CH_3 rock, CH_2 rock, C-C str (1-19;3-4;4-5;7-8;7-37;8-9;8-41;37-38), C-N str (1-21)
238	920(+)	915	919(–)	CH_3 rock, C-C str (1-2;1-29;2-3;2-26;12-13;12-46;12-47;13-14)
234	905(+)	890	895s(+) 890(+)	CH_3 rock, C-C str (7-37;37-38;8-9;6-7;8-41;9-10;12-46), Co-N str (22;23)
232	890(+)			CH_3 rock, CH_2 rock, C-C str (1-2;1-19;1-20;3-4;4-5;5-35;6-7;7-8;7-36;31-32), C-N str (1-21)
224	863(+)	849	-	C-C str (37-38;7-36;7-37;6-7;8-41;12-46;12-47), Co-N str (22) CH_3 rock, NH_2 rock

221	846(+)		837(+)	C-C str (60-61;42-43;8-9;12-46;12-47;11-12;13-48;31-32;10-11;48-49), CH_3 rock, CH_2 rock, NH_2 rock
212	811(+)	817s	823(+)	C-C str (49-50;48-49;13-48;12-47;12-13), C-N str (61-63), CH_2 rock, NH_2 rock
211	800(+)	792	799(+)	C-H bend out of plane (10)
205	767(+)	769s	-	CH_3 rock,CH_2 rock, C-C str (37-38;6-7;7-36;8-9), Co-N str (22)
203	749(+)	732	732(+)	CH_3 rock,CH_2 rock, corrin ring tors and bend
194	720(+)			corrin ring tors and bend, benzimidazole C-C str
190	707(+)			CH_2 rock, NH_2 twist, CCC bend, CC, CN tors
186	672(+)	696	695(–)	CH_2 rock, NH_2 twist, corrin ring tors and bend , CCC bend, CC, CN tors
177	627(+)	636	635(+)	NH_2 twist, corrin ring tors and bend
173	607(+)			NH_2 twist, corrin ring bend
168	584(+)	584	585(+)	NH_2 twist
165	560(+)	557	558(+)	NH_2 twist, corrin ring tors and bend
164	557(+)			corrin ring tors and bend, CCN, CNC bend, CC, CN tors
152	498(+)	518	518(+)	corrin ring tors and bend, NH_2 twist, CCC bend, CC, CN tors
148	482(–)	496	497(–)	Co-C≡N bend, C≡N twist, O-H bend (7R), benzimidazole ring breathing, Co-N bend (B3)
147	481(–)			Co-C≡N bend, C≡N twist, O-H bend (7R), benzimidazole ring breathing, Co-N bend (B3)
146	479(–)			Co-C≡N bend, C≡N twist, corrin ring tors and bend
144	468(+)	427	429(+)	Co-C≡N bend, corrin ring tors and bend, CCN, CNC bend, CC, CN tors
142	461(+)			Co-C≡N bend, C≡N twist, corrin ring tors and bend, CCN, CNC bend, CC, CN tors, O-H bend (7R)
141	459(+)			C≡N twist, corrin ring tors and bend, CCN, CNC bend, CC, CN tors, O-H bend (7R)
129	420(+)	404	408(+)	CCN, CNC bend, CC, CN tors, Co-N str (23;24)
125	402(+)			C≡N twist, Co-N str (22;23;24), CCN, CNC bend, CC, CN tors

Abbreviations: str – stretching; bend – bending; sym – symmetric; asym – asymmetric; wagg – wagging; twist – twisting; rock – rocking; tors – torsion; s – shoulder, (+) and (–) – positive and negative ROA intensities, numbers in brackets denotes atoms involved in vibrations accordingly to the Scheme 1 numeration.

Detailed characteristics of ECD and UV-vis spectra of cobalamins

UV-Vis absorption spectra of cobalamin species can be categorized as so-called "unique" (*i.e.* MeCbl, AdoCbl) or "typical" (CNCbl)[7,8] depending on the intensity and width of the α/β and γ bands assigned mostly to the corrin-based π→π* transitions along the long C5--C15 and short Co--C10 axis of the macrocycle, respectively.[8,9] The OH-substituted cobalamin exhibits the electronic spectrum in-between the "unique" and "typical". In the case of non-alkylcobalamins, like CNCbl, the UV-Vis absorption spectrum is characterised by two major features. First is the α/β band with the more intense counterpart at 550 nm and less intense at 521 nm being the electronic origin and vibrational progression, respectively, of the electronic excitation from the orbital HOMO to the orbital LUMO of the corrin ring. The second feature is the γ band in the near-ultraviolet region arising from several excitations involving molecular orbitals with dominating corrin π→π* nature.[8,10] The γ region results generally from mixing between Co 3d and corrin-based π orbitals that produces destabilization of all 3d orbitals.[8,11]

The detailed assignment of the UV-Vis and ECD spectra is given elsewhere.[7,8,10] Nevertheless, in the light of further considerations it is important to underline here the differences in the electronic spectra of studied cobalamins. In particular, previous thorough analysis demonstrated that UV-Vis spectrum of CNCbl in the α/β range exhibited vibrational progression of a single electronic transition (at 550 nm, 521 nm, 481 nm, Figure S5: band a, a', a" respectively), contrarily to alkylcobalamins that showed two bands due to two electronic transitions (at 525 and 495 nm).[8]

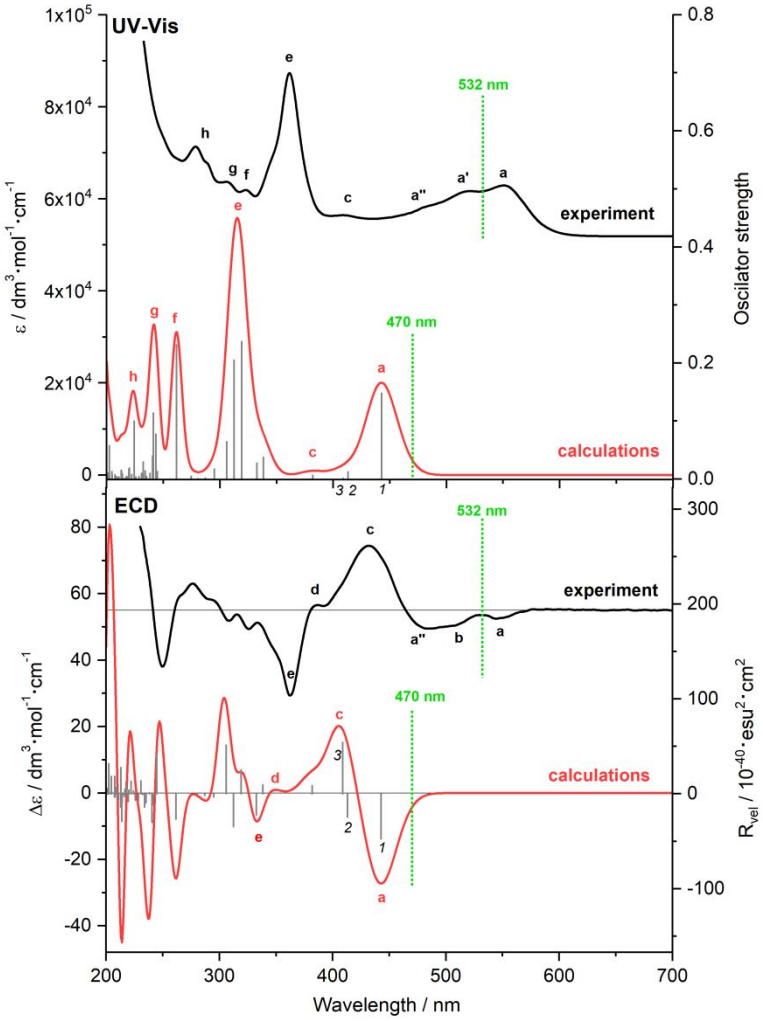

Figure S5. Comparison of experimental (black) and calculated (red) UV-Vis and ECD spectra of CNCbl, combined with calculated transition energies and their oscillatory and rotatory strengths (black vertical lines). Experimental and theoretical incident light wavelengths used in the Raman/ROA calculations are marked by green dotted lines.

Nevertheless, experimental ECD spectrum of CNCbl possessed two minima assigned to two distinct transitions at 550 (band a) and 507 nm (band b of null intensity in the UV-Vis absorption spectrum), and the minimum at 483 nm assigned to the vibrational progression (band a").[8] Experimental UV-Vis and ECD spectra of CNCbl correspond relatively well in the α/β spectral region with our simple theoretical TD-DFT model, apart from vibrational progression of the

first electronic state that is not taken into account in the vertical approximation calculations. Similarly to the experiment, two transitions (1 and 2) of the lowest energy (443 and 413 nm) have negative rotatory strengths, and the second one possess a rather weak UV-Vis intensity. Nevertheless, the energy of the transition 2 is underestimated in calculations and close to the nearby transition 3 (409 nm) with positive rotatory strength (Figure S5, Table S3). As it was mentioned, first electronic transition has mostly corrin ring $\pi \rightarrow \pi^*$ nature. However, molecular orbitals involved in the second (negative ECD) and third (positive ECD) electronic transitions of CNCbl are composed also by CN-π, DMB-π and Co 3d orbitals (Table S4, Figure S6). Experimental spectra below α/β region are also reproduced well by calculations, however ECD band assignment below 300 nm is not so straightforward as for UV-Vis (Figure S5). Predicted energies of electronic transitions are underestimated at the chosen theory level, however, in order to show relationship of incident light wavelength used to record experimental ROA/Raman spectra (*vide infra*), on position of the predicted electronic transitions, final theoretical electronic spectra were not shifted to fit the experimental results.

Table S3. Calculated energies (in nm), oscillator strengths (f) and rotatory strengths (R_{vel}) of first 10 electronic transitions of CNCbl calculated at CAM-B3LYP/6-31G(d)/MDF10/6-31G(d)/PCM theory level.

state	λ / nm	f	R_{vel} / 10^{-40}·esu^2·cm^2
1	442.70	0.1481	-47.4091
2	413.05	0.0127	-24.6200
3	408.90	0.0013	54.2751
4	381.76	0.0067	8.4658
5	338.35	0.0377	9.4751
	332.57	0.0276	-22.3948
6			
7	319.13	0.237	25.3162
8	312.30	0.2052	-34.5242
9	305.94	0.0646	51.2440
10	295.03	0.0172	-3.2797

For OHCbl, the shape of ECD is considerably different in comparison to CNCbl, with two bands of the opposite sign exhibited in the α/β range (Figure 1, manuscript). That significant differences in ECD between CNCbl and OHCbl is caused by different character of studied ligands. CN^- is a moderate *σ*-donor and strong *π*-acceptor, while OH^- is a weak *σ*-donor and strong *π*-donor that influences the electronic properties of the corrin ring. It is also reflected by the hipsochromic shift of the α/β and γ absorption bands of OHCbl compared to CNCbl that is associated with a well-known trend, where "typical" Cbl absorption spectra shift to higher energy with decreasing *σ*-donor strength of the upper axial ligand.[8]

These differences in the electronic absorption impact significantly on resonance conditions and have an impact on observed RROA spectra (*vide infra*). ECD spectra are very sensitive on the upper axial substituent what was related to electronic coupling of the axial ligand and the corrin

macrocycle.[7] Replacing of a CN^- group with a bulky $HC{\equiv}C{-}Ph{-}C{\equiv}C^-$ group has lower effect on UV-Vis and ECD signals than replacement with OH^- (Figure 1, manuscript).

Table S4. Dominant molecular orbital (MO) excitations along with energies (in nm), oscillator strengths (f) and rotatory strengths (R_{vel}) of the first 3 electronic transitions of CNCbl calculated at CAM-B3LYP/6-31G(d)/MDF10/6-31G(d)/PCM theory level.

state	λ / nm	f	R_{vel}	excitation	%	donor MO	acceptor MO
1	442.70	0.1481	-47.4091	354→355	88	cor-π (HOMO)	cor-π* (LUMO)
2	413.05	0.0127	-24.6200	320→357	11	cor-π/CN-π/Co $3d_{xy}$	Co $3d_{z^2}$/cor-π*/CN- π*
				352→357	11	cor-π/DMB-π/Co $3d_{xz}$	Co $3d_{z^2}$/cor-π*/CN- π*
3	408.90	0.0013	54.2751	323→357	12	cor-π/CN-π/Co $3d_{xz}$	Co $3d_{z^2}$/cor-π*/CN- π*

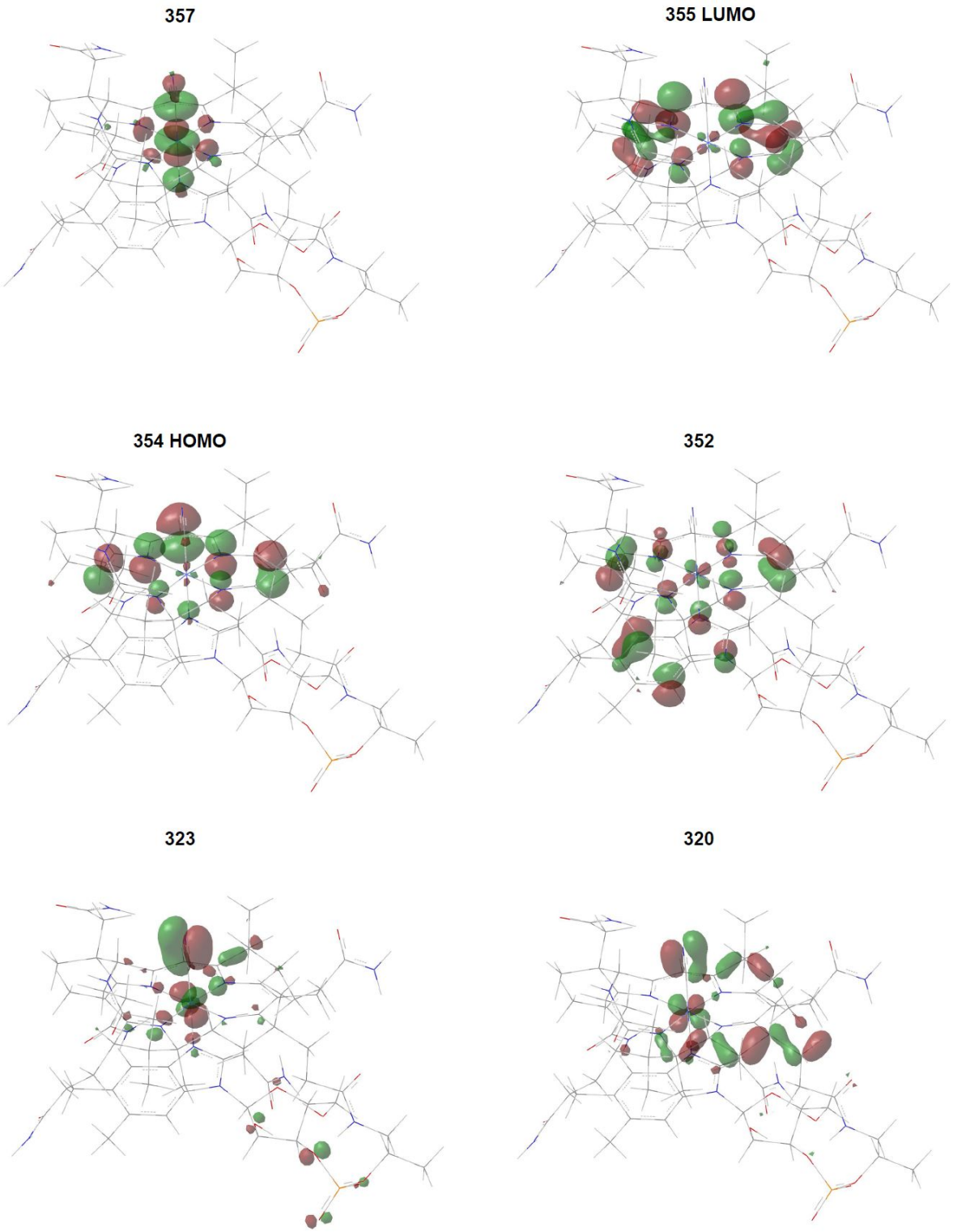

Figure S6. Molecular orbital contours, dominant in the first 3 electronic states of CNCbl calculated at CAM-B3LYP/6-31G(d)/MDF10/6-31G(d)/PCM theory level, convoluted in the GaussView 6 software.

g-factor values for obtained ECD and UV-vis spectra are given in Table S5.

Table S5. Dissymmetry factor (*g*-factor, ECD/UV-vis) values, plotted for selected transitions, obtained from CNCbl, OHCbl, HC≡C-Ph-C≡CCbl and CNCbl-Br experimental spectra.

CNCbl		OHCbl		HC≡C-Ph-C≡CCbl		CNCbl-Br	
λ / *nm*	g / 10^{-4}	λ / *nm*	g / 10^{-4}	λ / *nm*	g / 10^{-4}	λ / *nm*	g / 10^{-4}
544	-2.4	551	-5.5	552	-7.1	576	-0.8
507	-0.5	524	2.5	520	-1.3	569	-0.2
521	-2.3	513	3.7	448	32	552	0.9
483	-8.5	495	2.7			492	9.5
433	50	422	-46			435	59

Detailed characteristics of RR and RROA spectra of cobalamins

Calculated Raman and ROA spectra (Figure S7; Raman/ROA band assignment given in Table S2) are in good agreement with experimental results. Computed pre-resonance ROA and Raman spectra (470 nm excitation line), similarly to the experimental resonance spectra, show one dominant in intensity band at around 1500 cm^{-1}, and other low intensity transitions with similar to experiment relative intensities, except the spectral region below 1000 cm^{-1}, where computed intensities are visibly lower. Calculated ROA signals, in agreement with the experimental ones, are predominantly of the positive sign, i.e. opposite in sign to the ECD in the region of ROA excitation line, due to the close proximity of electronic transitions with the negative rotatory strengths (Figure S7).

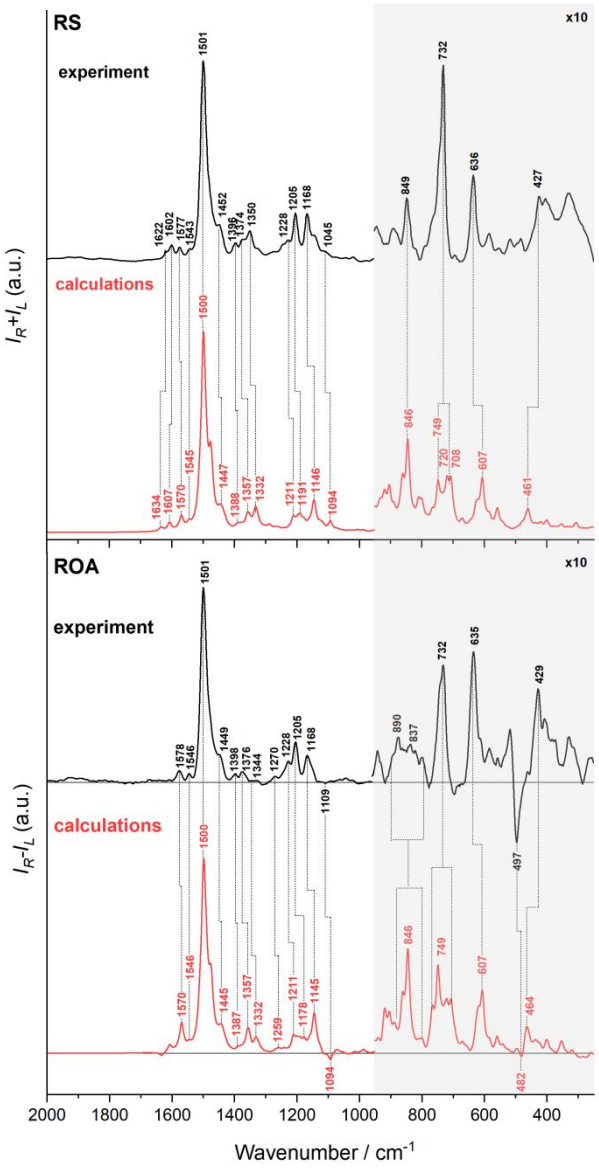

Figure S7. Comparison of experimental (black) and calculated (red) Raman and ROA spectra of CNCbl. Calculated frequencies were multiplied by a factor of 0.9446 to fit to the experimental ones.

Interestingly, calculations of the pre-resonance ROA spectra results also in signals of the negative intensity, in particular bands at 1094 and 482 cm^{-1} (in experimental spectrum at 1109 and 497 cm^{-1}, respectively), confirming that obtained ROA spectra of cobalamins are, indeed, bisignate. We calculated the preresonance Raman/ROA spectra also using other excitation lines (Figure 3, manuscript). The closer the excitation line is to the first electronic state (443 nm, negative ECD), that more monosignate (positive) ROA is. For 400 nm and 420 nm lines we do see bisignate ROA spectra due to close proximity of two electronic transitions (2 and 3) with opposite in sign rotatory strengths; while for the ROA spectra calculated at 650 nm excitation line, CNCbl is rather in the far from resonance conditions, that gives also bisignate ROA spectrum. Moreover, we do observe selective ROA intensity enhancement of vibrations specific for chromophore related with the electronic transition that is close by to the excitation laser line. Both 2nd (413 nm) and 3rd (409 nm) electronic transitions have similar cor-π/CN-π/Co 3d

character, but they possess opposite in sign ECD. Theoretical ROA, calculated at 420 nm line (close to the 2nd transition) and 400 nm line (close to the 3rd transition), are in some part of the spectra opposite in sign to each other, and, additionally, ROA intensity of vibrations due to Co-CN, and CN are more enhanced than the others.

CID values for obtained ROA and Raman spectra are given in Table S6.

Table S6. CID (ROA/Raman) values, plotted for selected transitions from CNCbl, OHCbl, HC≡C-Ph-C≡CCbl and CNCbl-Br experimental spectra.

CNCbl		OHCbl		HC≡C-Ph-C≡CCbl		CNCbl-Br	
v / cm^{-1}	*CID* / 10^{-4}	v / cm^{-1}	*CID* / 10^{-4}	v / cm^{-1}	*CID* / 10^{-4}	v / cm^{-1}	*CID* / 10^{-4}
1578	4.1	1578	4.0	1545	5.7	1561	1.3
1501	4.3	1501	4.5	1501	3.8	1522	3.3
1452	3.2	1447	3.1	1447	3.6	1476	4.6
1376	1.9	1367	7.2	1376	2.2	1392	10
1310	-3.3	1355	5.9	1354	-2.6	1364	20
1205	3.6	1203	2.2	1207	4.1	1336	-4.3
1168	2.4	1168	3.2	1168	1.6	1203	3.2
732	2.2	735	1.3	730	3.0	1161	2.2
636	5.7	637	4.6	636	3.7	1108	4.3
497	-40	516	3.5	486	6.0	815	7.4
427	6.1	493	-14	455	-11	728	2.6
		431	1.4	392	8.5	639	16
		395	-1.9			520	9.6
						500	-46
						468	82
						396	4.0

References

(1) Prieto, L.; Rossier, J.; Derszniak, K.; Dybas, J.; Oetterli, R. M.; Kottelat, E.; Chlopicki, S.; Zelder, F.; Zobi, F. Modified Biovectors for the Tuneable Activation of Anti-Platelet Carbon Monoxide Release. *Chem. Commun.* **2017**, *53* (51), 6840–6843.

(2) Rossier, J.; Nasiri Sovari, S.; Pavic, A.; Vojnovic, S.; Stringer, T.; Bättig, S.; Smith, S. G.; Nikodinovic-Runic, J.; Zobi, F. Antiplasmodial Activity and In Vivo Bio-Distribution of Chloroquine Molecules Released with a 4-(4-Ethynylphenyl)-Triazole Moiety from Organometallo-Cobalamins. *Molecules* **2019**, *24* (12).

(3) Frisch, M. J.; Trucks, G. W.; Schlegel, H. B.; Scuseria, G. E.; Robb, M. A.; Cheeseman, J. R.; Scalmani, G.; Barone, V.; Petersson, G. A.; Nakatsuji, H.; Li, X.; Caricato, M.; Marenich, A.; Bloino, J.; Janesko, B. G.; Gomperts, R.; Mennucci, B.; Hratchian, H. P.; Ortiz, J. V.; Izmaylov, A. F.; Sonnenberg, J. L.; Williams-Young, D.; Ding, F.; Lipparini, F.; Egidi, F.; Goings, J.; Peng, B.; Petrone, A.; Henderson, T.; Ranasinghe, D.; Zakrzewski, V. G.; Gao, J.; Rega, N.; Zheng, G.; Liang, W.; Hada, M.;

Ehara, M.; Toyota, K.; Fukuda, R.; J. Hasegawa; Ishida, M.; Nakajima, T.; Honda, Y.; Kitao, O.; Nakai, H.; Vreven, T.; Throssell, K.; J. A. Montgomery, J.; Peralta, J. E.; Ogliaro, F.; Bearpark, M.; Heyd, J. J.; Brothers, E.; Kudin, K. N.; Staroverov, V. N.; Keith, T.; Kobayashi, R.; Normand, J.; Raghavachari, K.; Rendell, A.; Burant, J. C.; Iyengar, S. S.; Tomasi, J.; Cossi, M.; Millam, J. M.; Klene, M.; Adamo, C.; Cammi, R.; Ochterski, J. W.; Martin, R. L.; Morokuma, K.; Farkas, O.; Foresman, J. B.; Fox, D. J. *Gaussian 09, Revision E.01*; Gaussian, Inc: Wallingford CT, 2016.

(4) Prieto, L.; Neuburger, M.; Spingler, B.; Zelder, F. Inorganic Cyanide as Protecting Group in the Stereospecific Reconstitution of Vitamin B_{12} from an Artificial Green Secocorrinoid. *Org. Lett.* **2016**, *18* (20), 5292–5295.

(5) Dennington, R.; Keith, T. A.; Millam, J. M. GaussView, Version 6.1. Semichem Inc: Shawnee Mission, KS 2016.

(6) O'boyle, N. M.; Tenderholt, A. L.; Langner, K. M. Cclib: A Library for Package-Independent Computational Chemistry Algorithms. *J. Comput. Chem.* **2008**, *29* (5), 839–845.

(7) Brunold, T. C. Combined Spectroscopic/computational Studies of Metal Centers in Proteins and Cofactors: Application to Coenzyme B_{12}. *Chimia (Aarau).* **2004**, *58* (4), 186–193.

(8) Stich, T. A.; Brooks, A. J.; Buan, N. R.; Brunold, T. C. Spectroscopic and Computational Studies of Co^{3+}-Corrinoids: Spectral and Electronic Properties of the B_{12} Cofactors and Biologically Relevant Precursors. *J. Am. Chem. Soc.* **2003**, *125* (19), 5897–5914.

(9) Salama, S.; Spiro, T. G. Visible and Near-ultraviolet Resonance Raman Spectra of Photolabile Vitamin B_{12} Derivatives with a Rapid-flow Technique. *J. Raman Spectrosc.* **1977**, *6* (2), 57–60.

(10) Park, K.; Brunold, T. C. Combined Spectroscopic and Computational Analysis of the Vibrational Properties of Vitamin B_{12} in Its Co^{3+}, Co^{2+}, and Co^{1+} Oxidation States. *J. Phys. Chem. B* **2013**, *117* (18), 5397–5410.

(11) Reig, A. J.; Conrad, K. S.; Brunold, T. C. Combined Spectroscopic/computational Studies of Vitamin B_{12} Precursors: Geometric and Electronic Structures of Cobinamides. *Inorg. Chem.* **2012**, *51* (5), 2867–2879.